THE ASTROPHYSICAL JOURNAL, 458:455–466, 1996 February 20

THE STELLAR HALO OF M104. I. A SURVEY FOR PLANETARY NEBULAE AND THE PLANETARY NEBULA LUMINOSITY FUNCTION DISTANCE

H. C. FORD[1]
Physics and Astronomy Department, Johns Hopkins University, Charles and 34th Streets, Baltimore, MD 21218; and Space Telescope Science Institute

X. HUI[1,2]
Astronomy Department, California Institute of Technology, 105-24, Pasadena, CA 91125

R. CIARDULLO[3]
Department of Astronomy and Astrophysics, Pennsylvania State University, 525 Davey Lab, University Park, PA 16802

G. H. JACOBY
Kitt Peak National Observatory, National Optical Astronomy Observatories, P.O. Box 26732, Tucson, AZ 85726-6732

AND

K. C. FREEMAN
Mount Stromlo and Siding Spring Observatories, Australian National University, Private Bag, Weston Creek Post Office, ACT 2611, Australia

Received 1993 August 17; accepted 1995 August 22

ABSTRACT

We used the CTIO 4 m telescope to make a complete and kinematically unbiased survey of M104 (NGC 4594; the Sombrero galaxy) for planetary nebulae (i.e., stars) out to 16 kpc. We present the positions and monochromatic [O III] λ5007 magnitudes of 294 planetaries, and use the observed planetary nebula luminosity function (PNLF) to measure a distance of 8.9 ± 0.6 Mpc to the galaxy. The luminosity-specific PN number $\alpha_{2.5}$ in the halo of M104 is approximately $21.7 \times 10^{-9}\ L_{\odot}$, which for its color $(B-V) = 0.95$, is comparable to the values in other galaxies.

We use the PNLF distance to M104 to compare its luminosity to the luminosities of the brightest galaxies in the Virgo Cluster, finding that if M104 were in the Virgo Cluster, it would be the third brightest galaxy. We combined the PNLF distance and the observed velocity corrected for Virgo infall to calculate a Hubble constant $H_0 = 91 \pm 8$ km s^{-1} Mpc^{-1}. We also used the PNLF distances to the NGC 1023 group, the Leo group, the Virgo Cluster, and the Fornax Cluster to derive Hubble constants corrected for Virgo infall.

The values of H_0 for M104, the NGC 1023 group, the Virgo Cluster, and the Fornax Cluster are in excellent agreement, suggesting that the PNLF distances and Schechter's linear infall model provide a self-consistent representation of the Hubble expansion and Virgo infall within most regions of the local supercluster. The unweighted mean of the four values is $H_0 = 84 \pm 4$. The value of H_0 derived for the Leo group differs by four standard deviations from the mean of the other four measurements. We conclude that there may be large peculiar motions in the spatially extended Leo spur.

Subject headings: distance scale — galaxies: clusters: individual (Virgo) — galaxies: distances and redshifts — galaxies: individual (M104) — galaxies: stellar content — planetary nebulae: general

1. INTRODUCTION

The Sombrero galaxy (NGC 4594 or M104) is a conspicuous Sa galaxy with a prominent bulge and a highly inclined disk. The galaxy has been the subject of kinematic studies at many wavelengths (Faber et al. 1977; Schweizer 1978; Kormendy & Illingworth 1982; Bajaja et al. 1984; Rubin et al. 1985; Kormendy & Westpfahl 1989). Using integrated absorption spectra, Kormendy & Illingworth (1982) measured the rotation and velocity dispersion of the bulge at several position angles. Subsequently, Jarvis & Freeman (1985) successfully fitted an isotropic oblate model to their data, confirming that the bulge is an oblate spheroid for which the flattening is due mostly to rotation, but with a small contribution from the disk potential. This result is consistent with the picture that the bulges of spiral galaxies are oblate rotators.

Absorption-line spectroscopy is hampered by the rapid falloff of the surface brightness beyond a galactic distance of 80″. To probe the halo kinematics and mass distribution of the galaxy, one has to rely on other test particles. Recent work by Bridges & Hanes (1992) revealed that the galaxy has a rich population of globular clusters. The globular cluster system is spatially more extended and metal poorer than the halo stars, suggesting that the globular cluster halo is older than the stellar halo. M104 also has an extended X-ray corona (Forman, Jones, & Tucker 1985). Based on the X-ray studies, the estimated total mass within a galactic radius of 16 kpc[4] is $8.9 \times 10^{11}\ M_{\odot}$. The corresponding circular velocity is 480 km s^{-1}, whereas the observed H I velocity is 370 km s^{-1} at 9 kpc. The difference may indicate that the X-ray data overestimate

[1] Visiting Astronomer, Cerro Tololo Inter-American Observatory, operated by the Association of Universities for Research in Astronomy, Inc., under contract with the National Science Foundation.
[2] Hubble Fellow.
[3] 1992 NSF Young Investigator.
[4] We adopt 8.9 Mpc for the distance to M104. At this distance, the scale is 2.6 kpc per arcmin.

the total mass, but the comparison is not really valid because the characteristic radius of the X-ray emission is about twice the extent of the H I clouds.

The stellar halo of the Sombrero galaxy can be studied directly by using planetary nebulae (PNs). Unlike their K giant precursor stars, PNs can be detected in the halos of galaxies to the distance of the Virgo Cluster (Jacoby, Ciardullo, & Ford 1990, hereafter J90), and can yield accurate radial velocities at distances of at least 10 Mpc. A recently completed study of NGC 5128 illustrates the effectiveness of using planetaries to study stellar dynamics. Hui (1992) and Hui et al. (1993a, b) identified nearly 800 PNs in that galaxy out to a galactic distance of 20 kpc or 4 effective radii, a fourfold increase in radius compared to conventional observations of elliptical galaxies using absorption line spectra. Hui (1992) and Hui et al. (1995) subsequently measured the radial velocities of over 400 nebulae. These unique data were used to explore the halo dynamics and mass distribution in an early-type galaxy for the first time. We plan to make similar studies of halos around other early-type galaxies, and begin with the Sombrero galaxy. The halo PN study, combined with the rotation curve of the disk, will significantly improve our understanding of the stellar kinematics and the mass distribution in M104. The comparison of the kinematics of the stellar halo (i.e., PNs) and the globular cluster halo will cast light on the formation and evolution of the galaxy.

The planetary nebular luminosity function (PNLF) is also an important standard candle for early-type galaxies. The foundation for this recently established distance indicator lies in the observed bright cutoff of the PNLF, as first noted in Local Group galaxies by Ford & Jenner (1979). The steep falloff of the PNLF was further studied in the bulge of M31 (Ciardullo et al. 1989b) and was shown to have the same shape in 25 galaxies which included giant ellipticals in the Virgo Cluster, the bulge of M81, and two late-type, metal-poor galaxies, the LMC and the SMC (Ciardullo, Jacoby, & Ford 1989a; Jacoby et al. 1989; J90; Jacoby, Walker, & Ciardullo 1990; Ciardullo, Jacoby, & Harris 1991; Hui et al. 1993a). Comparison of the PNLF distances to different galaxies in the same group or cluster show that the distances have a high relative accuracy. The PNLF distances to M81 (Jacoby et al. 1989) and the LMC (Jacoby et al. 1990) are the same as the Cepheid distances to these galaxies. PNLF distances also are in excellent agreement with distances derived from surface brightness fluctuations. Nonetheless, some workers (Bottinelli et al. 1991) question the validity of PNLF distances. Consequently, PNLF distances to additional galaxies should either reinforce the claimed accuracy, or reveal population and sample-dependent systematic errors. As a relatively nearby, early-type spiral galaxy with a prominent bulge, M104 provides us with an opportunity to better understand any possible systematic differences between the PNLFs in different types of galaxies.

We used the CTIO 4 m telescope to make a spatially complete and kinematically unbiased survey of M104's halo for PNs. We found 294 PNs in the survey region, which extends out to 16 kpc along the photometric major axis and to 13 kpc along the photometric minor axis. Using the Anglo-Australian 4 m telescope and a multifiber spectrograph, we measured the radial velocities of ~150 of the planetaries. The spectroscopic observations and a detailed dynamical study of the M104 halo will be the subject of a subsequent paper. In this first paper we present the survey for PNs and use the PNLF to derive an accurate distance to M104.

The paper is arranged as follows. We present the observations in § 2 and the PN positions and monochromatic [O III] λ5007 magnitudes in § 3. In § 4, we use the observed PNLF to measure the distance to M104 and the luminosity-specific PN number. In § 5, we first compare various distance measurement to M104; we then use the new PNLF distance to compare M104's luminosity to the luminosities of the brightest galaxies in the Virgo Cluster. Finally, we use M104's PNLF distance and observed velocity corrected for infall into the Virgo Cluster to calculate the Hubble constant H_0, which we compare to the Hubble constants derived from the PNLF distances to the NGC 1023 group, the Leo group, the Virgo Cluster, and the Fornax Cluster.

2. OBSERVATIONS

The PN survey was made with a Texas Instruments 800 × 800 CCD (no. 1) at the f/2.77 prime focus of the CTIO 4 m telescope. The gain of the CCD was set to 1.4 electrons per analog-to-digital unit, and the CCD readout noise was 6.5 electrons per pixel. Given the scale of 0.″3 per 15 μm pixel at the focal plane, the CCD provided a 4′ × 4′ field. During three clear nights, we imaged seven fields using on-band/off-band [O III] λ5007 interference filters. The on-band images were typically exposed for 3 hr. The survey area (Fig. 1) extends to 7.′4 along the photometric major axis and to 5.′7 along the minor axis. As shown in the figure, we overlapped the fields so that photometric and astrometric errors caused by shot noise, variable seeing, and changes in transparency could be estimated. The detailed observing log is given in Table 1, where the last two columns are the effective airmass (Stetson 1989) for the total exposure and the average seeing (FWHM) in the summed images. The table does not include the off-band exposures, which were always one-eighth the on-band exposure times.

We took several exposures of photometric standard stars at the beginning and end of each night. Because the CCD had a

TABLE 1

M104 Planetary Nebula Survey

UT Date	Field	α (2000)	δ (2000)	Exposure Time (s)	Airmass	FWHM
1990 Mar 25.....	17	$12^h39^m37^s.5$	−11°37′25″	3 × 3600	1.22	1.″4
	14	12 40 21.8	−11 37 26	3 × 3600	1.26	1.3
1990 Mar 26.....	16	12 39 52.2	−11 37 26	2 × 1800, 2 × 3600	1.19	1.1
	15	12 40 08.0	−11 37 27	2 × 3600, 3000	1.25	1.1
1990 Mar 27.....	22	12 39 52.2	−11 33 50	3 × 3600	1.43	1.5
	21	12 40 07.5	−11 33 52	2 × 3600	1.08	1.3
	10	12 39 53.0	−11 41 08	4200	1.41	1.4

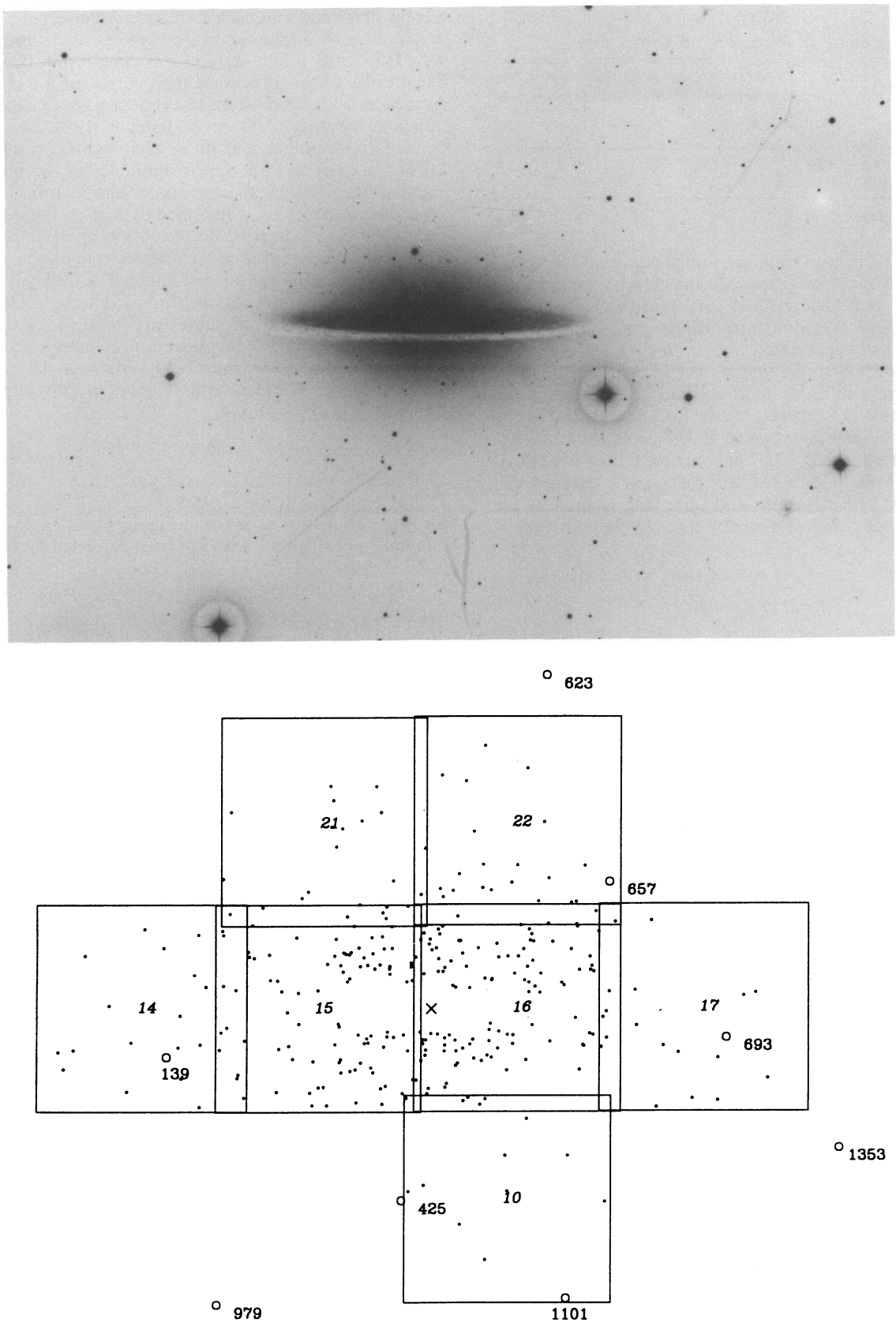

FIG. 1.—The top panel shows a plate of M104 taken by A. Sandage with the Palomar 5 m telescope. The bottom panel shows the survey fields plotted to the same scale as the 5 m plate. The numbered filled circles are GSC stars (see Table 6). The open boxes are the positions of the planetary nebulae. The big cross marks the center of M104. The apparent void in the distribution along the equatorial plane is due to the conspicuous dust lane.

TABLE 2

INTERFERENCE FILTERS USED FOR THE M104 SURVEY

FILTER DESIGNATION	λ_c/FWHM f/2.77	λ_c/FWHM f/13	MAXIMUM TRANSMISSION (f/2.77) (%)
Andover 1157	5027/34[a]	5043/32	70
Andover 1455	5310/262	...	90

[a] At the ambient temperature of 11° C.

small amount of charge trapping for backgrounds less than ~30 counts per pixel, we preflashed the chip before the short exposures of standard stars. The survey exposures were not preflashed because the long integrations gave sufficient sky counts for good charge transfer.

The characteristics of the interference filters used to isolate the PNs are given in Table 2. In the f/2.77 converging beam and at the ambient temperature of 11° C, the central wavelength of the on-band filter was at 5027 Å, well suited for the M104 PNs, whose [O III] λ5007 lines are redshifted to approximately 5025 Å at M104's systemic velocity. A detailed discussion of filter considerations and observing techniques are given in Ford et al. (1989) and Jacoby et al. (1989).

3. DATA REDUCTION

3.1. *CCD Reductions*

The CCD images were reduced by first subtracting the average of 25 bias frames and then dividing by the average of five dome flats taken through the corresponding filter. By dividing a dome flat into a twilight image, we concluded that the illumination of the dome flat was uniform to 0.25%–0.5%. We also estimated that the residual Poisson noise in the flat fields was about 1%. The CCD images of the same field were registered and added before blinking each on-band and off-band pair to identify the PNs. Cosmic rays were removed during the addition. A stellar object was classified as a PN candidate if it appeared only in the on-band image, but not in the off-band image. A total of 294 PN candidates were detected in the seven fields.

The PN instrumental magnitudes and their (x, y) positions were measured using a point spread function (PSF) fitting procedure in the IRAF.DAOPHOT software package. A PSF was constructed for each frame by combining several carefully preselected bright stars. The measurements were made directly on the [O III] λ5007 on-band images of the halo fields, but not on the two central fields 15 and 16, wherein the rapid change in the galaxy background degraded the photometric precision. We created a galaxy background model for the latter two fields by first subtracting bright stars with a scaled PSF and then highly smoothing the image with a filter designed to remove faint objects and any other high-frequency structures. The smoothed image was subtracted from the [O III] λ5007 on-band frame and the PSF fitting was done in the difference images. Experiments showed that this procedure did not introduce any additional random noise. The photometric errors in the two central fields were similar to the errors in the halo fields.

3.2. [O III] λ5007 *Flux Calibration*

The PN instrumental magnitudes were transformed into [O III] λ5007 fluxes in the following steps. First, the PN instrumental magnitudes in each frame were converted to aperture magnitudes by adding aperture corrections determined from several isolated bright stars in the same frame. The aperture magnitudes of the PNs were then corrected for atmospheric extinction using a CTIO mean extinction coefficient $A_{\lambda 5030} = 0.19$ mag airmass^{-1} (Stone & Baldwin 1983, SB). Next, we derived a zero point constant for each night by comparing the extinction-corrected aperture magnitudes of the photometric standard stars to their spectral energy distributions following a procedure similar to one described by Jacoby, Quigley, & Africano 1987. The extinction-corrected PN aperture magnitudes were finally converted to monchromatic magnitudes by adding the zero point constant for each night. The transmission curve of the interference filter was incorporated in the last step.

The PNs found in our survey are listed in Table 3, where column (1) gives the PN identification, columns (2) and (3) give the PN coordinates in the J2000 system of the Guide Star Catalog (see § 3.3) and column (4) gives the PN luminosity in the equivalent V magnitude

$$m_{5007} = -2.5 \log (\text{flux}) - 13.74 , \quad (1)$$

where "flux" is in units of ergs cm^{-2} s^{-1} (Ciardullo et al. 1989b). Note that the first two digits of the PN identification is the field designation as given in Figure 1 and Table 1. The PN luminosities in Table 3 have not been corrected for foreground galactic extinction.

Throughout the first night thin cirrus could be seen from the horizon up to an elevation of ~20° from the southwest through west, and occasionally in the north. On the second night cirrus was visible on the horizon in the south through the west at the beginning of the night. At no time during the first two nights were we able to see high cirrus, and we concluded that these nights were photometric. During the course of the third night cirrus could be seen as high as 60°. However, continuous photoelectric observations on another telescope showed that the changes in the transparency during the third night did not exceed 1%–2% (Buie 1990), a variation which should have a negligible effect on the flux measurements.

Nevertheless, we took two approaches to look for possible systematic errors in the [O III] λ5007 fluxes caused by variations in the transparency. Table 4 gives the zero point constants in magnitudes for each exposure of the standard stars and the average zero point correction for each night. The standard deviations for the second and third nights were 0.02 mag, which is comparable to the internal consistency of the standard star fluxes (see SB). Although the standard deviation (0.05 mag) for the first night is more than twice the value of the other nights, the means for the three nights agree to better than 0.01 mag. Because the CCD detectors are highly stable, the excellent agreement in the zero points suggests that the observations were photometric to ~1%.

We also checked our observations by comparing the magnitudes of stars and PNs in the common regions of the seven overlapping fields (Fig. 2). The average difference is Δ mag = -0.003 ± 0.022 except for the common stars between fields 16 and 22, where Δ mag = 0.20 ± 0.03. Because no systematic error is seen in comparing field 16 with other fields, we conclude that the average magnitudes of stars in field 22 are 0.2 mag brighter than the stars in the other fields. Field 22 was observed during the third night at a large airmass of 1.44. If the observations were affected by cirrus, the stars in field 22 would be too faint rather than too bright. Because we could not identify the cause of the discrepancy, we excluded the stars in

TABLE 3

M104 PLANETARY NEBULAE

ID	$\alpha(2000)$	$\delta(2000)$	m_{5007}	ID	$\alpha(2000)$	$\delta(2000)$	m_{5007}
1001	12 39 56.717	−11 41 37.95	25.60	1536	12 40 09.612	−11 37 09.43	26.07
1002	12 39 45.226	−11 41 10.91	25.69	1537	12 40 05.826	−11 36 23.93	26.07
1003	12 39 54.699	−11 42 18.13	25.76	1540	12 40 05.693	−11 36 56.36	26.09
1004	12 39 48.150	−11 40 17.74	25.91	1541	12 40 06.612	−11 36 06.70	26.10
1005	12 39 52.946	−11 40 59.33	26.06	1542	12 40 06.209	−11 38 41.46	26.11
1006	12 40 00.779	−11 41 00.04	26.09	1543	12 40 02.478	−11 37 54.89	26.11
1007	12 39 53.114	−11 40 17.82	26.11	1544	12 40 01.195	−11 37 58.28	26.14
1008	12 39 51.407	−11 39 34.31	26.25	1545	12 40 06.345	−11 37 48.82	26.15
1009	12 39 59.571	−11 40 52.88	26.37	1546	12 40 08.408	−11 38 29.16	26.15
1401	12 40 22.677	−11 38 06.96	25.47	1547	12 40 04.353	−11 38 08.53	26.16
1402	12 40 20.177	−11 36 16.75	25.57	1548	12 40 00.990	−11 39 11.36	26.18
1403	12 40 15.722	−11 37 55.44	25.65	1549	12 40 05.560	−11 36 24.67	26.21
1404	12 40 17.802	−11 36 47.63	25.68	1551	12 40 00.196	−11 38 49.87	26.25
1405	12 40 17.464	−11 36 01.80	25.92	1552	12 40 11.144	−11 38 14.37	26.25
1406	12 40 26.278	−11 36 25.71	25.96	1553	12 40 10.905	−11 37 07.82	26.26
1407	12 40 17.357	−11 38 09.45	25.98	1554	12 40 13.264	−11 35 50.28	26.26
1408	12 40 18.820	−11 38 48.34	26.24	1555	12 40 00.543	−11 36 35.50	26.26
1409	12 40 21.672	−11 35 55.21	26.25	1556	12 40 14.562	−11 37 06.01	26.26
1410	12 40 14.345	−11 38 43.97	26.31	1557	12 40 13.488	−11 36 26.82	26.32
1411	12 40 14.989	−11 35 37.33	26.43	1558	12 40 06.348	−11 38 29.96	26.33
1412	12 40 27.187	−11 38 15.83	26.45	1561	12 40 03.659	−11 38 41.84	26.40
1413	12 40 15.824	−11 38 15.65	26.48	1562	12 40 05.997	−11 36 22.27	26.40
1414	12 40 27.952	−11 38 37.95	26.59	1563	12 40 03.648	−11 36 23.37	26.40
1415	12 40 19.034	−11 38 12.82	26.60	1564	12 40 09.734	−11 36 04.93	26.40
1416	12 40 18.900	−11 37 36.04	26.62	1565	12 40 11.256	−11 36 55.07	26.43
1417	12 40 15.525	−11 36 02.11	26.63	1567	12 40 05.001	−11 39 16.07	26.48
1418	12 40 28.358	−11 38 18.36	26.70	1568	12 40 13.903	−11 39 10.34	26.49
1419	12 40 17.390	−11 39 20.91	26.74	1569	12 40 00.599	−11 36 33.94	26.50
1420	12 40 15.270	−11 37 50.17	26.74	1570	12 40 06.025	−11 36 44.01	26.50
1421	12 40 24.385	−11 37 24.52	26.80	1571	12 40 02.287	−11 36 46.74	26.51
1422	12 40 22.966	−11 39 03.29	26.89	1572	12 40 04.387	−11 36 28.02	26.54
1423	12 40 16.890	−11 37 02.14	27.10	1573	12 40 04.778	−11 36 16.86	26.55
1502	12 40 02.007	−11 38 00.89	25.22	1574	12 40 03.079	−11 36 36.33	26.56
1503	12 40 02.791	−11 38 12.47	25.38	1575	12 40 04.679	−11 36 37.88	26.57
1504	12 40 00.504	−11 36 54.66	25.49	1576	12 40 11.340	−11 39 03.95	26.60
1505	12 40 06.241	−11 36 36.49	25.49	1577	12 40 03.005	−11 39 00.23	26.61
1506	12 40 05.494	−11 36 51.98	25.56	1578	12 40 02.090	−11 36 17.51	26.63
1507	12 40 00.592	−11 36 38.09	25.59	1579	12 40 02.901	−11 36 03.98	26.65
1509	12 40 03.525	−11 36 40.84	25.61	1580	12 40 04.138	−11 38 02.80	26.65
1510	12 40 10.033	−11 38 25.98	25.63	1581	12 40 02.297	−11 36 37.98	26.65
1511	12 40 13.850	−11 38 04.76	25.65	1582	12 40 06.715	−11 36 26.25	26.67
1512	12 40 00.921	−11 36 56.16	25.71	1583	12 40 14.450	−11 38 47.69	26.67
1513	12 40 00.432	−11 38 49.46	25.74	1584	12 40 07.601	−11 38 58.56	26.70
1514	12 40 03.803	−11 37 59.60	25.74	1585	12 40 02.319	−11 36 40.65	26.70
1515	12 40 04.641	−11 38 30.51	25.75	1586	12 40 05.389	−11 36 21.60	26.72
1516	12 40 03.721	−11 36 05.17	25.75	1587	12 40 04.074	−11 36 36.70	26.72
1517	12 40 02.146	−11 35 52.22	25.77	1589	12 40 02.742	−11 36 17.70	26.73
1518	12 40 11.830	−11 36 53.87	25.83	1590	12 40 08.494	−11 39 19.67	26.78
1519	12 40 11.917	−11 36 24.58	25.88	1591	12 40 10.334	−11 38 10.97	26.79
1520	12 40 04.026	−11 38 07.80	25.91	1592	12 40 08.704	−11 39 05.03	26.83
1521	12 40 05.488	−11 38 39.82	25.91	1593	12 40 13.580	−11 36 21.27	26.86
1522	12 40 08.031	−11 37 06.92	25.91	1594	12 40 00.863	−11 38 16.71	26.87
1523	12 40 06.683	−11 38 09.30	25.91	1595	12 40 05.059	−11 38 38.27	26.95
1524	12 40 04.830	−11 37 58.15	25.91	1596	12 40 13.113	−11 36 28.41	26.97
1525	12 40 05.188	−11 35 51.61	25.93	1597	12 40 15.517	−11 37 01.20	27.00
1526	12 40 06.410	−11 37 45.62	25.96	1598	12 40 07.322	−11 39 19.66	27.03
1527	12 40 00.206	−11 36 27.07	25.97	1599	12 40 15.595	−11 35 57.11	27.19
1528	12 40 09.545	−11 37 45.41	25.98	15100	12 40 06.241	−11 38 26.93	27.41
1529	12 40 02.657	−11 38 57.10	25.98	1601	12 39 58.493	−11 37 57.42	25.44
1530	12 40 02.536	−11 38 00.76	26.02	1602	12 39 57.742	−11 38 54.16	25.53
1531	12 40 03.792	−11 38 35.94	26.02	1603	12 39 54.413	−11 37 52.41	25.55
1532	12 40 08.019	−11 38 58.69	26.02	1604	12 39 53.784	−11 36 11.67	25.57
1533	12 40 07.299	−11 36 35.00	26.05	1605	12 39 58.072	−11 36 43.35	25.64
1534	12 40 01.262	−11 39 05.61	26.05	1606	12 39 59.304	−11 39 05.67	25.64
1535	12 40 02.893	−11 39 17.96	26.07	1607	12 39 51.254	−11 37 08.46	25.65

TABLE 3—*Continued*

ID	α(2000)	δ(2000)	m_{5007}	ID	α(2000)	δ(2000)	m_{5007}
1608	12 39 59.660	−11 38 08.41	25.65	1680	12 39 54.744	−11 36 51.74	26.56
1609	12 39 55.000	−11 38 28.02	25.66	1681	12 39 56.067	−11 39 10.03	26.57
1610	12 39 46.189	−11 37 58.03	25.67	1682	12 39 47.876	−11 36 17.82	26.57
1611	12 39 53.698	−11 38 13.32	25.68	1683	12 39 46.104	−11 36 42.67	26.59
1612	12 39 54.705	−11 39 11.73	25.69	1684	12 39 49.607	−11 38 05.64	26.59
1613	12 39 52.390	−11 36 45.32	25.70	1685	12 39 57.892	−11 38 58.35	26.60
1614	12 39 58.449	−11 36 43.54	25.73	1686	12 39 47.494	−11 35 48.72	26.60
1615	12 39 47.243	−11 36 41.08	25.74	1687	12 39 57.954	−11 38 16.53	26.62
1617	12 39 46.916	−11 38 10.65	25.78	1688	12 39 58.386	−11 36 28.85	26.64
1618	12 39 57.920	−11 38 09.85	25.78	1689	12 39 55.117	−11 39 17.74	26.64
1619	12 39 59.866	−11 37 54.91	25.81	1690	12 39 56.886	−11 35 40.07	26.64
1620	12 39 53.654	−11 36 27.51	25.82	1691	12 39 57.002	−11 38 16.91	26.65
1622	12 39 49.720	−11 35 48.13	25.83	1692	12 39 52.088	−11 36 26.20	26.66
1623	12 39 50.976	−11 37 46.53	25.84	1693	12 39 58.447	−11 35 55.27	26.66
1624	12 39 54.547	−11 38 21.55	25.86	1694	12 39 51.040	−11 36 00.40	26.66
1625	12 39 54.547	−11 38 21.55	25.86	1695	12 39 51.582	−11 36 53.69	26.67
1626	12 39 53.639	−11 37 54.15	25.86	1697	12 39 58.315	−11 36 00.47	26.72
1627	12 39 56.425	−11 39 14.10	25.87	1698	12 39 54.208	−11 36 53.68	26.73
1628	12 39 59.473	−11 38 21.53	25.88	1699	12 39 48.629	−11 36 56.43	26.75
1629	12 39 52.549	−11 38 08.57	25.91	16100	12 39 50.296	−11 36 45.51	26.78
1630	12 39 59.442	−11 38 15.83	25.94	16101	12 39 46.467	−11 37 56.23	26.82
1631	12 39 55.279	−11 36 16.59	25.95	16102	12 39 54.412	−11 38 04.88	26.83
1632	12 39 50.969	−11 36 31.04	25.96	16103	12 39 56.673	−11 36 08.55	26.84
1633	12 39 55.678	−11 38 03.23	25.97	16104	12 39 51.472	−11 38 26.94	26.84
1634	12 39 56.467	−11 38 13.56	25.97	16105	12 39 45.734	−11 35 57.10	26.86
1635	12 39 51.883	−11 35 49.76	26.00	16106	12 39 54.292	−11 37 45.24	26.87
1636	12 39 51.272	−11 36 56.96	26.02	16107	12 39 51.138	−11 36 07.78	26.90
1637	12 39 46.426	−11 36 26.26	26.02	16108	12 39 48.441	−11 37 00.04	26.94
1638	12 39 51.235	−11 35 54.74	26.02	16109	12 39 49.356	−11 36 09.67	26.98
1639	12 39 59.196	−11 38 59.60	26.03	16110	12 39 46.262	−11 36 36.52	27.02
1640	12 39 46.968	−11 38 09.60	26.03	16112	12 39 58.087	−11 35 51.51	27.04
1641	12 39 52.975	−11 37 58.02	26.04	16113	12 39 50.878	−11 36 09.00	27.05
1642	12 39 47.542	−11 37 38.58	26.08	16114	12 39 57.287	−11 37 00.79	27.10
1643	12 39 52.915	−11 36 26.29	26.09	16115	12 39 51.372	−11 36 37.57	27.18
1644	12 39 59.005	−11 37 56.79	26.10	16116	12 39 47.247	−11 38 38.02	27.45
1645	12 39 51.680	−11 36 18.01	26.12	16117	12 39 47.405	−11 35 51.73	28.15
1646	12 39 59.160	−11 36 12.40	26.12	1701	12 39 41.224	−11 39 20.40	25.50
1647	12 39 54.192	−11 38 23.72	26.13	1702	12 39 40.716	−11 38 10.07	25.76
1649	12 39 56.494	−11 36 22.72	26.18	1703	12 39 44.891	−11 37 07.04	25.80
1650	12 39 58.937	−11 36 19.05	26.19	1704	12 39 44.466	−11 35 46.14	25.80
1651	12 39 46.378	−11 36 41.33	26.20	1705	12 39 39.552	−11 38 17.86	25.87
1652	12 39 52.519	−11 37 58.33	26.23	1706	12 39 45.558	−11 38 11.74	26.02
1653	12 39 57.086	−11 38 04.65	26.26	1707	12 39 42.896	−11 37 05.50	26.13
1654	12 39 59.806	−11 38 28.00	26.26	1708	12 39 41.645	−11 35 44.47	26.16
1655	12 39 50.746	−11 37 01.47	26.28	1709	12 39 45.142	−11 38 01.19	26.19
1656	12 39 56.205	−11 36 37.79	26.29	1710	12 39 45.409	−11 37 37.47	26.26
1657	12 39 59.586	−11 36 46.40	26.30	1711	12 39 38.447	−11 39 10.39	26.47
1658	12 39 55.919	−11 38 09.12	26.30	1712	12 39 42.796	−11 37 46.82	26.56
1659	12 39 50.404	−11 37 08.70	26.30	1713	12 39 36.429	−11 39 12.95	26.66
1660	12 39 59.849	−11 36 07.07	26.33	1714	12 39 36.445	−11 38 24.09	26.90
1661	12 39 53.011	−11 38 38.35	26.34	1715	12 39 45.148	−11 37 30.46	26.94
1663	12 39 59.434	−11 38 03.97	26.35	1716	12 39 34.419	−11 37 11.58	26.96
1664	12 39 56.907	−11 38 30.72	26.42	1717	12 39 33.489	−11 37 08.30	26.97
1665	12 39 57.898	−11 36 38.89	26.42	1718	12 39 32.529	−11 38 47.43	27.01
1666	12 39 59.095	−11 36 06.53	26.43	2101	12 40 03.380	−11 33 10.26	25.45
1667	12 39 56.803	−11 36 08.50	26.43	2102	12 40 02.562	−11 35 29.67	25.57
1668	12 39 57.895	−11 38 01.91	26.43	2103	12 40 02.048	−11 34 58.92	25.66
1669	12 39 57.421	−11 36 31.48	26.44	2104	12 40 06.625	−11 34 18.99	25.66
1670	12 39 59.652	−11 38 04.10	26.44	2105	12 40 07.049	−11 33 09.32	25.75
1671	12 39 54.173	−11 36 52.08	26.46	2106	12 40 03.019	−11 33 39.41	25.80
1672	12 39 57.044	−11 38 33.59	26.46	2107	12 40 00.861	−11 35 28.28	25.86
1673	12 39 57.028	−11 37 02.98	26.46	2108	12 40 04.550	−11 33 48.72	25.88
1674	12 39 57.546	−11 37 58.27	26.47	2109	12 40 05.697	−11 35 40.79	25.97
1675	12 39 55.615	−11 38 25.13	26.48	2110	12 40 02.847	−11 35 36.14	26.02
1676	12 39 58.582	−11 36 16.73	26.49	2111	12 40 09.348	−11 35 18.84	26.12
1677	12 39 59.589	−11 35 59.57	26.53	2112	12 40 08.825	−11 35 11.93	26.13
1679	12 39 55.930	−11 37 03.08	26.54	2113	12 40 04.698	−11 35 26.94	26.22

TABLE 3—*Continued*

ID	α(2000)	δ(2000)	m_{5007}
2114	12 40 02.587	−11 35 43.04	26.33
2115	12 40 12.432	−11 35 29.90	26.35
2116	12 40 15.516	−11 34 56.74	26.36
2117	12 40 06.838	−11 33 25.48	26.41
2118	12 40 14.912	−11 33 38.78	26.62
2119	12 40 06.974	−11 33 56.20	26.86
2120	12 40 06.111	−11 33 57.61	26.89
2201	12 39 49.653	−11 34 55.65	25.24
2202	12 39 45.971	−11 35 33.88	25.56
2203	12 39 59.505	−11 34 20.66	25.62
2204	12 39 56.255	−11 33 03.22	25.63
2205	12 39 58.127	−11 32 56.96	25.65
2206	12 39 58.057	−11 35 17.32	25.71
2207	12 39 59.802	−11 35 14.34	25.84
2208	12 39 54.877	−11 34 39.48	25.96
2209	12 39 56.784	−11 34 50.81	25.97
2210	12 39 54.941	−11 35 06.94	25.98
2211	12 39 52.171	−11 34 40.25	25.99
2212	12 39 54.240	−11 35 09.56	26.01
2213	12 39 55.610	−11 34 01.24	26.14
2214	12 39 58.283	−11 35 07.97	26.19
2215	12 39 51.366	−11 32 49.06	26.19
2216	12 39 54.746	−11 32 23.56	26.28
2217	12 39 50.053	−11 33 50.27	26.40
2218	12 39 52.609	−11 35 00.53	26.43
2219	12 39 46.834	−11 34 40.75	26.47
2220	12 39 47.503	−11 35 22.94	26.54
2221	12 39 50.494	−11 35 22.23	26.55
2222	12 39 57.283	−11 35 10.09	26.69
2223	12 39 47.891	−11 35 23.93	27.30

field 22 from the PNLF analysis. With this exclusion we conclude that our observations were not affected by cirrus.

Based on a comparison of the magnitudes of the PNs and stars in the common regions, we estimate that the PN luminosities are accurate to 9% (1 σ) in the range of $m_{5007} = 25$–27. This empirical estimate is consistent with the errors in Table 5,

TABLE 4

THE NIGHTLY ZERO POINT CONSTANT

Standard Star	Zero Point Constant	Airmass	Exposure (s)
EG 54	17.98	1.04	50
LTT 4364	17.97	1.40	10
LTT 6248	18.09	1.07	10
LTT 7379	18.04	1.06	2
EG 274	18.07	1.03	4
Night one average	18.03 ± 0.03		
EG 54	18.05	1.03	50
LTT 3864	18.05	1.13	25
LTT 6248	18.05	1.05	10
LTT 7379	18.01	1.06	2
LTT 7379	18.05	1.06	4
EG 274	18.06	1.02	4
Night two average	18.04 ± 0.01		
EG 54	18.02	1.03	50
LTT 3864	18.02	1.29	25
LTT 3864	18.02	1.23	25
LTT 4364	18.02	1.62	15
LTT 6248	18.08	1.06	10
LTT 7379	18.01	1.06	4
EG 274	18.05	1.02	4
EG 274	18.07	1.03	8
Night three average	18.04 ± 0.01		

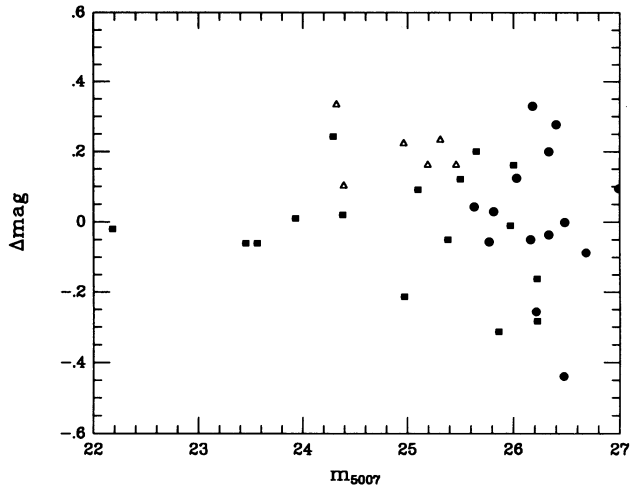

FIG. 2.—Magnitude differences of stars (*squares*) and PNs (*dots*) found in the common regions of the overlapping fields vs. their apparent magnitudes, m_{5007}. Triangles are stars in the common region between fields 16 and 22.

TABLE 5

PN PHOTOMETRIC ERROR VS. m_{5007}

m_{5007}	Number of Planetary Nebulae	σ
25.14.....	3	0.047
25.45.....	6	0.048
25.64.....	37	0.049
25.88.....	53	0.059
26.11.....	55	0.076
26.37.....	59	0.086
26.63.....	56	0.099
26.87.....	27	0.113
27.07.....	11	0.126
27.39.....	3	0.257

which were calculated by averaging the DAOPHOT 1 σ errors in 0.2 mag intervals.

3.3. *PN Coordinates*

We used the Guide Star Catalog (GSC) and the related software system at the Space Telescope Science Institute to measure the PN coordinates in the J2000 system. Because each CCD frame is only 4′ × 4′ on the sky, there are few stars with cataloged positions in our survey fields. Consequently, we used GSC software and plate solutions to measure the right ascensions and declinations of those stars (defined as secondary reference stars) appearing on both the digitized sky survey plate and the CCD frames. On average, about five stars could be measured in each CCD image. To improve the accuracy of the astrometric solution, we used the stars in the common regions to tie all fields (except no. 10) together. The CCD images were shifted into a common coordinate system without rotation between different frames. With 33 stars distributed uniformly across the survey area, we obtained a satisfactory astrometric solution which models shift, scaling, and rotation between the CCD frames and the sky survey plate. The 1 σ error of the solution is about 0.″6 in each coordinate. We estimate that the overall accuracy of the PN positions should be better than 0.″3 in each coordinate relative to the GSC stars in Table 6 or the secondary reference stars in Table 7. The data in Table 6 were taken directly from the GSC catalog, where the coordinates are typically accurate to 0.″3 in right ascension and declination.

TABLE 6

GSC STARS IN THE M104 FIELD

ID	α(2000)	δ(2000)	Mag
633.....	12h40m07s.84	−11°27′57″.0	11.05
623.....	12 39 49.92	−11 30 19.3	12.60
545.....	12 40 58.17	−11 31 43.1	10.76
1061.....	12 39 06.25	−11 33 15.7	12.83
1343.....	12 40 56.70	−11 34 52.3	12.48
1353.....	12 39 26.94	−11 40 08.4	11.09
1160.....	12 40 40.22	−11 42 14.6	12.89
979.....	12 40 16.01	−11 43 10.3	10.45
872.....	12 39 11.17	−11 43 29.6	12.36
1025.....	12 40 23.11	−11 48 39.7	11.20
327.....	12 40 11.39	−11 49 49.6	9.68
950.....	12 39 06.95	−11 49 54.5	12.18
657.....	12 39 44.92	−11 34 59.5	14.65
693.....	12 39 35.77	−11 38 00.4	15.10
139.....	12 40 19.97	−11 38 23.7	13.07
425.....	12 40 01.36	−11 41 10.4	15.05
1101.....	12 39 48.32	−11 43 03.0	15.36

TABLE 7

SECONDARY REFERENCE STARS

ID	α(2000)	δ(2000)
S1001.....	12h39m48s.31	−11°43′03″.1
S1002.....	12 39 46.23	−11 41 37.9
S1003.....	12 39 46.65	−11 43 02.4
S1401.....	12 40 25.25	−11 38 41.1
S1403.....	12 40 27.67	−11 36 22.1
S1405.....	12 40 19.84	−11 37 45.7
S1501.....	12 40 01.21	−11 38 41.7
S1505.....	12 40 14.53	−11 38 27.9
S1509.....	12 40 15.52	−11 36 20.8
S1601.....	12 39 51.73	−11 35 58.3
S1603.....	12 39 45.25	−11 36 00.4
S1606.....	12 39 50.08	−11 38 29.0
S1701.....	12 39 42.20	−11 37 16.3
S1703.....	12 39 39.40	−11 39 08.0
S1704.....	12 39 38.89	−11 37 27.4
S2103.....	12 40 02.22	−11 33 13.8
S2104.....	12 40 00.05	−11 32 48.5
S2108.....	12 40 14.85	−11 34 20.1
S2201.....	12 39 52.48	−11 32 18.2
S2202.....	12 39 51.84	−11 35 14.7
S2203.....	12 39 47.43	−11 34 22.0

4. THE PNLF DISTANCE TO M104

The PNLF follows an empirical form

$$\Phi(m) \propto e^{0.307m}[1 - e^{3(m^* - m)}] , \quad (2)$$

where m^* defines the bright cutoff of the PNLF (Ciardullo et al. 1989b). The absolute magnitude of m^* is equal to −4.48 if, as we assume in this paper, M31 is at a distance of 710 kpc (Welch et al. 1986) and has a differential extinction $E(B-V) = 0.11$. If instead we use the Cepheid distance to M31 derived by Freedman & Madore (1990) and the foreground extinction from Burstein & Heiles (1982), all PNLF distances increase by 3% and all derived values of the Hubble constant decrease by 3%.

The PNLF distance of a galaxy can be derived by fitting the above function to the observed PNLF using a maximum likelihood method. The program gives the most likely solution for the distance modulus and the luminosity specific PN number (the scaling factor for $\Phi[m]$).

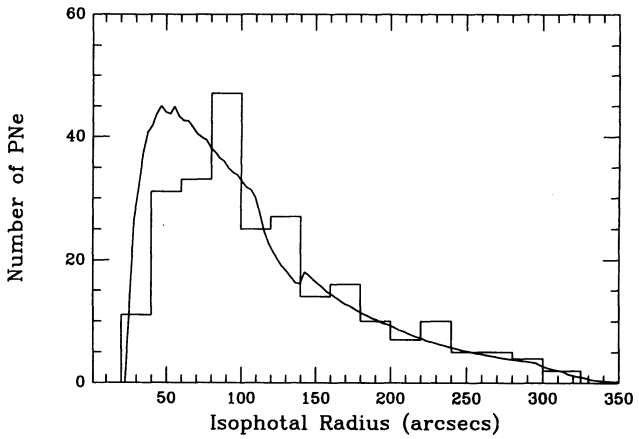

FIG. 3.—The PN distribution as a function of isophotal radius. The continuous curve superposed on the histogram is the light distribution sampled in the survey fields.

In order to derive the PNLF distance, we first must define a statistically uniform and complete PN sample. PNs surveys in distant galaxies are typically complete in the brightest first magnitude. The limiting magnitude for our sample can be determined by comparison with the PNLF in the bulge of M31, where incompleteness does not begin until 2 mag below the cutoff (Ciardullo et al. 1989b). The limiting magnitude varies with radius in the bright central region of the galaxy, and becomes a constant only when the sky background dominates the light in the halo. The variation of the limiting magnitude may be examined by comparing the distribution of planetary nebulae with that of the galaxy light encompassed in the survey frames (Fig. 3). In calculating the equivalent isophotal radius for each PN and each pixel of the CCD frames, we take the axial ratio of the isophotes to be 0.7, and the photometric minor axis to be at P.A. = 0°. We further assume that the surface brightness profile along the photometric minor axis is

$$\mu_V = 2.74r^{1/4} + 13.09 , \quad (3)$$

where r has units of arcsecs (Jarvis & Freeman 1985). The central 400″ × 50″ region, which is obscured by the dust lane, is excluded here and in the subsequent analysis. Figure 3 shows that the PN number (the histogram) follows the light distribution (*solid curve*) beyond 80″, suggesting that the limiting magnitude is a constant at large radii. In the inner region, however, there is an increasing deficiency of PNs caused by a progressively brighter limiting magnitude and possibly by increasing metallicity in the parent stellar population. Consequently, we divide the M104 PNs into sample A, which includes all the PNs inside of an equivalent isophotal radius of 80″, and sample B which includes all PNs with radii greater than 80″.

We also calculate the total bolometric luminosity in our survey fields, namely the normalization in the luminosity specific PN number. First, we estimate the apparent V light to be 9.69 and 10.02 mag for samples A and B, respectively. Using the assumed foreground extinction of $E(B-V) = 0.028$ (Burstein & Heiles 1982) and a Seaton (1979) reddening law, the reddening corrected magnitudes are 9.59 and 9.92. Next we combine the near-infrared observation of Wainscoat, Hyland, & Freeman (1990) and the photoelectric surface photometry of Wirth (1981) and de Vaucouleurs (1960) to derive the following apparent *UBVRIJHK* colors: $V-J = 1.86$, $V-H = 2.63$,

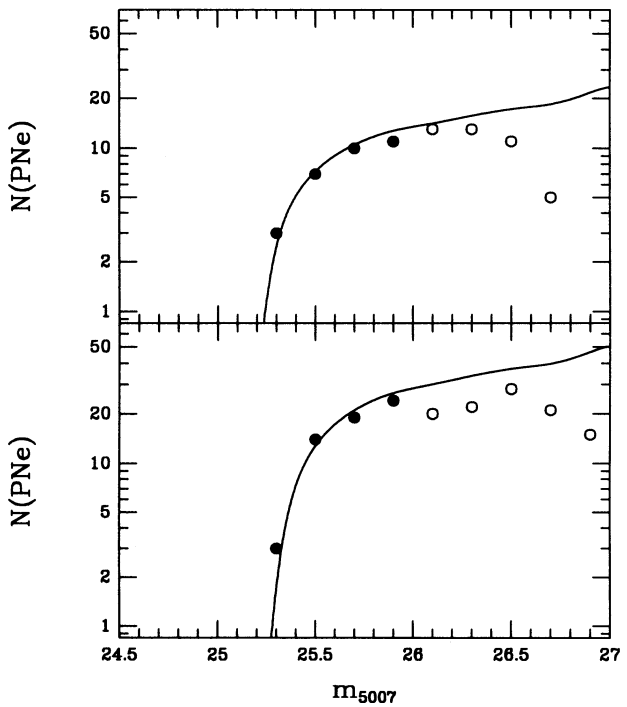

FIG. 4.—The M104 PNLFs for sample A (*upper panel*) and sample B (*lower panel*). The data are binned into 0.2 mag intervals. The solid curves are the convolution of the empirical PNLF with the mean photometric error vs. magnitude relation; the convolved curves were translated to the most likely distance modulus of the galaxy. Open circles show PNs below the completeness limit; these PNs were not included in the fits.

$V-K = 2.88$, $B-V = 0.98$, $V-R = 0.88$, $R-I = 0.76$, and $U-B = 0.525$. Because of the color gradient in the galaxy, all colors are estimated at 100″ along the photometric minor axis except $U-B$, which is the integrated color within $r = 1'.77$, corrected for internal reddening. Finally, we estimated the bolometric correction to be -0.87 by integrating the energy distribution implied by the broadband colors. This value is similar to that found for M31 (Ciardullo et al. 1989b) and the giant ellipticals of Virgo (J90). The resulting total bolometric luminosity m_{bol} is 8.72 and 9.05 for samples A and B.

The PNLFs for the two samples are shown in Figure 4. Also shown are the best fitting functions, which are equation (3) convolved with the PN photometric errors taken from Table 5. We adopted a completeness magnitude $m_{5007} = 26.0$ (Fig. 4) for both samples; there are 61 PNs in sample A and 32 PNs in sample B brighter than this magnitude. The most likely solutions for the two samples are given in Table 8; the derived distances are highly consistent. Finally, we combine the two samples for our best estimate of the distance modulus, $29.74^{+0.04}_{-0.06}$. Combining the uncertainties in the distance of the calibration galaxy M31 (0.1 mag), the foreground extinction (0.05 mag), the PNLF model (0.05 mag), and the filter calibration (0.05 mag), the overall error in the M104 distance is 0.14 mag, or 7%. Consequently, the best estimate of the PNLF distance to M104 is 8.9 ± 0.6 Mpc.

TABLE 8

MAXIMUM LIKELIHOOD SOLUTIONS

Sample	$(m-M)_0$	$\alpha_{2.5} \times 10^9$
A	$29.70 + 0.06/-0.12$	14.2 ± 4.0
B	$29.77 + 0.07/-0.07$	21.7 ± 4.8

There is one PN candidate, no. 1502, which is brighter than any other PN in M104 by 0.16 mag. We investigated the likelihood that no. 1502 is the result of a chance fluctuation at the bright end of the PNLF by running Monte Carlo simulations in which we drew PNs from our adopted PNLF. Effects of the 0.05 mag uncertainty in the photometry were included in the simulations. A difference as large as 0.16 mag between the first and second brightest PNs occurred ~7% of the time. We tentatively reject no. 1502 from the maximum likelihood fitting procedure on the grounds that it is not likely to be a member of the characteristic sample, although only at the 2σ level. Including it has the effect of reducing the distance to M104 by $\leq 4\%$.

Slightly overluminous "PNs" like no. 1502 can arise by a chance superpositions of two PNs. If this effect were modeled by the reference PNLF in the maximum likelihood fit, the change in distance to M104 by including or excluding no. 1502 would be insignificant. A spectrum of no. 1502 obtained with the Anglo-Australian Telescope shows a strong emission line at 5019.52 Å, which is redshifted [O III] λ5007 from the bright planetary. The second strongest feature in the spectrum is a "line" at ~5002.9 Å which stands approximately 1σ above the noise and has a strength between 30% and 50% of the brightest line. The transmission of our on-band interference filter at this wavelength is ~10%. The line, if real, would increase the brightness of no. 1502 by ~0.05 to 0.07 mag. If this second line is [O III] λ5007 from a PN in M104, its observed velocity is 4–5 standard deviations from M104's systemic velocity. We conclude that no. 1502 is not a superposition of two PNs.

Table 8 also lists the luminosity specific PN number $\alpha_{2.5}$, which is defined as the PN number in the first 2.5 mag of the PNLF normalized to the bolometric luminosity. The halo specific number $\alpha_{2.5}$ and the halo color $(B-V) = 0.95$ follow closely the $\alpha_{2.5}$-color relation defined by other galaxies (Hui et al. 1993a, Fig. 12). The luminosity specific PN number falls by approximately 35% for the inner region (sample A). A similar phenomenon was observed in NGC 5128 (Hui et al. 1993a). It is likely that the same population effect gives rise to both the $\alpha_{2.5}$-color relation among galaxies and the $\alpha_{2.5}$ gradient within a galaxy.

5. DISCUSSION

5.1. *Comparison with Other Distance Measurements*

Several efforts have been made to derive the distance to M104. Earlier studies include the *B*-band or *V*-band Faber-Jackson relation (de Vaucouleurs & Olson 1982), and the *B*-band Tully-Fisher relation (de Vaucouleurs 1983; Bottinelli et al. 1984). Based on these papers, the average distance modulus to the galaxy is $(m-M)_0 = 30.02 \pm 0.19$ (de Vaucouleurs 1993a). Using a new and better value from the RC3 for the total luminosity of the galaxy, de Vaucouleurs (1992) revised the earlier measurements, and obtained $(m-M)_0 = 29.73 \pm 0.13$. Using the surface brightness fluctuation method, Tonry (1992) estimated that the distance modulus of the galaxy is $(m-M)_0 = 29.65$. Within the statistical errors, both numbers are consistent with the PNLF distance $(m-M)_0 = 29.74 \pm 0.14$. The average of the three independent measurements results in the best estimate of the M104 distance modulus $(m-M)_0 = 29.71 \pm 0.03$.

Bridges & Hanes (1992) used the globular cluster luminosity

function (GCLF) to measure the distance to M104. They found that if the Milky Way GCLF is adopted as the calibrator, the distance modulus of the galaxy is $(m - M)_0 = 31.0 \pm 0.35$, which is 1.29 mag larger than the above best estimate $(m - M)_0 = 29.71 \pm 0.03$. However, if the GCLF is compared to that of the giant ellipticals in Virgo, and the Virgo distance modulus is $(m - M)_0 = 30.8 \pm 0.20$, the GCLF distance modulus to M104 is $(m - M)_0 = 30.0 \pm 0.25$. In the latter case, the difference is reduced to 0.29 mag. These differences possibly may be resolved by the new GCLF fitting technique used by Secker & Harris (1993).

5.2. *The Luminosity of M104*

We can use our PNLF distance to calculate the luminosity of M104 and to compare its luminosity to other bright galaxies. The first two columns in Table 9 were taken from the Third Reference Catalogue of Bright Galaxies (de Vaucouleurs et al. 1991; RC3) and give M104's observed blue magnitude and the blue magnitude corrected for internal and galactic extinction. The third column was taken from the Revised Shapley Ames Catalog (Sandage & Tammann 1981; RSA), and is the absolute magnitude derived by dividing M104's recessional velocity of 1089 km s^{-1} reduced to the centroid of the Local Group ($v_0 = 873$ km s^{-1}) by the Hubble constant of 50 km s^{-1} Mpc^{-1} assumed in the RSA. The last column in Table 9 gives the extinction-corrected absolute blue magnitude derived from our PNLF distance of 8.9 Mpc. Our absolute magnitude is 1.5 mag fainter than the RSA value, which is based on a Hubble distance of 17.5 Mpc to M104.

We compare M104 to luminous galaxies in the Virgo Cluster by adding the difference in the respective distance moduli to M104's observed magnitude. We minimize the systematic errors in the comparison by using PNLF distances and assuming J90's well-determined PNLF distance of 14.7 ± 1.0 Mpc to the Virgo Cluster. Table 10 lists the five brightest galaxies in the RSA which satisfy Huchra's (1985) velocity and positional criteria for membership in the Virgo Cluster. The only bias in the sample is the fact that the five galaxies are in a cluster. The galaxy types are from the RSA and the observed magnitudes B_T, and extinction-corrected magnitudes B_T^0 are from the RC3. The last line gives the magnitudes M104 would have if it were at the distance of the Virgo Cluster. M104 is indeed a luminous galaxy, and would have the third brightest apparent magnitude were it in the Virgo Cluster. This is in contrast to the absolute magnitudes given in the RSA, which place M104 0.43 mag brighter than NGC 4472, the brightest galaxy in Virgo.

TABLE 9

ABSOLUTE MAGNITUDE OF M104

B_T (RC3) (1)	B_T^0 (RC3) (2)	$M_{B_T^{0,i}}$ (RSA) (3)	$M_{B_T^0}$ This Paper (4)
8.98.....	8.39	−22.81	−21.31

TABLE 10

COMPARISON OF M104 WITH THE BRIGHTEST GALAXIES IN THE VIRGO CLUSTER

Galaxy (NGC/Messier)	Type (RSA)	B_T (RC3)	B_T^0 (RC3)
N4472/M49	E1/S0$_1$(1)	9.37	9.26
N4486/M87	E0	9.59	9.47
N4569/M90	Sab(s)I–II	10.26	9.79
N4501/M88	Sbc(s)II	10.36	9.36
N4216	Sb(s)	10.99	10.03
N4594/M104.....	Sa$^+$/Sb$^-$	10.08[a]	9.49[a]

[a] Apparent magnitude at the distance of the Virgo Cluster.

5.3. *The Hubble Constant*

We can combine the PNLF distance to M104 and its observed radial velocity to measure the Hubble constant. A comparison of this value with values of H_0 derived from the PNLF distances to other groups and clusters within the Local Supercluster will show whether or not the PNLF distances and the model for Virgo infall within the Local Supercluster are self-consistent. In the subsequent analysis we will use the PNLF distances to the Virgo Cluster (J90), the Leo group (Ciardullo et al. 1989a), the NGC 1023 group (Ciardullo et al. 1991), and the Fornax Cluster (McMillan, Ciardullo, & Jacoby 1993). To calculate the Hubble constant, we begin with v_0, which is the observed heliocentric radial velocity v corrected to the centroid of the Local Group. The mean positions and mean velocities v_0 for the Leo and NGC 1023 groups were calculated (as explained below) using group members listed in the catalogs by Huchra & Geller (1982, hereafter HG82) and Tully (1987, hereafter T87). The mean position and observed heliocentric velocity for the Fornax Cluster were taken from Abell, Corwin, & Olowin (1989). We next calculate the angle θ between the center of the Virgo Cluster (Huchra 1985) and the group or galaxy, and use Schechter's (1980) linear model for Virgo infall, as expressed by equation (1) in Tammann & Sandage (1985), to calculate the velocity correction v_g which is the sum of the galaxy or group's infall to Virgo and the infall of the Local Group to Virgo v_{vc} projected onto the line of sight to the group. For consistency with J90, we adopt their mean value $v_{vc} = 253$ km s^{-1} for the infall of the Local Group into the Virgo Cluster. In the subsequent error analysis, we assume that the uncertainty in v_{vc} is ± 50 km s^{-1}. Finally, we calculate the "Hubble" velocity $v_H = v_0 + v_g$.

The NGC 1023 group has eight members in HG82's catalog (group no. 67). Excluding IC 0239, which differs from the mean of the remaining seven group members by 6 σ, the mean RSA v_0 is 824 km s^{-1}. The NGC 1023 group is no. 17-1 in T87 and includes the seven group members in HG82 plus an additional six faint galaxies. The mean v_0 for the 13 galaxies is 822 km s^{-1}. The two values are effectively identical, showing that this group is well defined in projection and in velocity space.

The three bright galaxies in Leo with PNLF distances (Ciardullo et al. 1989a) are members of group number 56 (30 galaxies) in HG82, and group 15-1 in T87 (nine galaxies). The discrepancy between the number of members assigned to the group reflects this region's spatial complexity. Tully (1987) decomposes the region into a foreground Leo spur, containing eight groups, and a background Leo cloud, consisting of 18 groups. HG82's group 56 includes six T87 groups. The mean v_0 for the 27 galaxies in HG82's group which have RSA velocities is 928 km s^{-1} with a velocity dispersion $\sigma = 272$ km s^{-1}. In contrast, the mean v_0 for the nine galaxies in T87's group is 618 km s^{-1} with a dispersion $\sigma = 120$ km s^{-1}. The large difference between the two values suggests that HG82's group 56 is not a single gravitationally bound group. Because T87's group 15-1 appears to be a separate entity both in projection and in veloc-

TABLE 11

VIRGO INFALL CORRECTIONS AND THE HUBBLE CONSTANT

PARAMETER	GALAXY GROUP				
	M104	Leo	NGC 1023	Virgo	Fornax
Mean heliocentric velocity, v (km s^{-1})	1089[a]	735[b]	589	1151[c]	1380[d]
Velocity corrected to LG centroid, v_0 (km s^{-1})	874 ± 50	631 ± 150	824 ± 28[e]	1035 ± 38	1289 ± 40
Infall correction, v_g (km s^{-1})	−62 ± 12	−104 ± 20	7 ± 1	253 ± 50	−50 ± 10
"Hubble" velocity, v_H (km s^{-1})	812 ± 51	526 ± 151	831 ± 28	1286 ± 63	1239 ± 41
Mean right ascension, $\langle\alpha\rangle$ (1950.0)	$12^h37^m.4$	$11^h03^m.0$	$2^h29^m.8$	$12^h27^m.8$	$3^h36^m.6$
Mean declination, $\langle\delta\rangle$ (1950.0)	−11°21′.0	14°59′	37°40′.3	12°56′	−35°37′
Angle θ between Virgo and galaxy/group (°)	24.4	20.5	121.9	...	132.0
PNLF distance (Mpc)	8.9 ± 0.6	10.1 ± 0.1	9.9 ± 0.5	14.7 ± 1.0	16.9 ± 1
Hubble constant, H_0 (km s^{-1} Mpc^{-1})	91 ± 8	52 ± 15	84 ± 4	87 ± 7	73 ± 5

[a] Sandage & Tammann 1981; RSA.
[b] Mean RSA heliocentric velocities for the nine members of T87's Leo Group 51-1.
[c] Huchra's 1985 mean velocity for 362 Virgo members.
[d] Abell, Corwin, & Olowin 1989.
[e] Mean RSA and HG82 velocities (v_0) for seven of HG82's members of the NGV 1023 Group (HG no. 67); IC 0239 was excluded from the mean.

ity space, we will use $v_0 = 618$ km s^{-1} for the mean velocity. Although the error in v_0 due to group assignment is not random, we will assume the uncertainty is ~150 km s^{-1}, which is half the difference between the two values.

The PNLF distances are the mean of distances to six galaxies in the Virgo Cluster (J90), three galaxies in the Leo group, two galaxies in the NGC 1023 group (Ciardullo et al. 1991), and three galaxies in the Fornax Cluster (McMillan et al. 1993). All quantities and their estimated uncertainty are given in Table 11. The formal errors in the values of the Hubble constant were calculated using standard procedures for error propagation (e.g., Bevington 1969). The uncertainty in v_0 for M104 should include the (small) error in the measurement of the radial velocity and the random motion of M104 relative to a smooth infall. We somewhat arbitrarily assumed that these combine to a total uncertainty of approximately ±50 km s^{-1}.

The values of H_0 derived from the PNLF distance measurements to M104, the NGC 1023 group, the Virgo Cluster, and the Fornax Cluster are in excellent agreement, differing by no more than their respective errors. The value of H_0 for the Leo group (51 ± 15 km s^{-1} Mpc^{-1}) differs by 4 σ from the mean of the other four values. Had we used $v_0 = 928$ km s^{-1} which we derived from HG82's assignments, the value of H_0 would have been 82 ± 15 km s^{-1} Mpc^{-1}. Although this would put H_0 in excellent agreement with the values derived for M104, the NGC 1023 group, Virgo, and Fornax, we think T87's assignments are more likely to represent a gravitationally bound group than HG82's much larger group. The discrepant value of H_0 is then caused by either an error in our PNLF distance to the Leo group, or by a large peculiar motion which is not described by Schechter's infall model. The standard deviation of the PNLF distances to the three galaxies in the Leo group was ~4% of the mean distance, and the total estimated error was ~10% (Ciardullo et al. 1989a). Consequently, we think the problem is more likely due to large peculiar motions in the spatially extended Leo spur. The large peculiar motions in this region were noted by Faber & Burstein (1988), and were attributed by them to the irregular distribution of galaxies in the Local Supercluster and the large-scale flow attributed to the "Great Attractor."

The unweighted mean of the Hubble constant derived from M104, the NGC 1023 group, Virgo, and Fornax is $H_0 = 84$ ± 4 km s^{-1} Mpc^{-1}. Although we excluded the Leo group for the reasons given above, had we included it, the mean value of the Hubble constant would be $H_0 = 77 \pm 7$ km s^{-1} Mpc^{-1}.

Our value of 84 ± 4 km s^{-1} Mpc^{-1} is in excellent agreement with de Vaucouleurs's (1993a) value of 87 ± 1 km s^{-1} Mpc^{-1} derived from an exhaustive analysis of all recent short distance scale determinations, and also agrees well with de Vaucouleurs's (1993b) value of 85 ± 4 km s^{-1} Mpc^{-1} derived from a new method based on the specific frequencies of globular clusters.

M104, the NGC 1023 group, the Virgo Cluster, and the Fornax Cluster sample widely differing distances and directions within the Local Supercluster. The consistency of the Hubble constant derived from these four measurements shows that PNLF distances and Schechter's linear infall model provide a self-consistent representation of the Hubble expansion and Virgo infall within most regions of the Local Supercluster.

This research was supported by NSF grant No. IRI-9116843.

REFERENCES

Abell, G. O., Corwin, H. G., Jr., & Olowin, R. P. 1989, ApJS, 70, 1
Bajaja, E., van der Burg, G., Faber, S. M., Gallagher, J. S., Knapp, G. R., & Shane, W. W. 1984, A&A, 141, 309
Bevington, P. R. 1969, Data Reduction and Error Analysis for the Physical Sciences (New York: McGraw-Hill), 62
Bottinelli, L., Gouguenheim, L., Paturel, G., & de Vaucouleurs, G. 1984, A&A, 56, 381
Bottinelli, L., Goughenheim, L., Paturel, G., & Teerikorpi, P. 1991, A&A, 252, 550
Bridges, T. J., & Hanes, D. A. 1992, AJ, 103, 800
Buie, M. 1990, personal communication
Burstein, D., & Heiles, C. 1982, AJ, 87, 1165
Ciardullo, R., Jacoby, G. H., & Ford, H. C. 1989a, ApJ, 344, 715
Ciardullo, R., Jacoby, G. H., Ford, H. C., & Neill, J. D. 1989b, ApJ, 339, 53
Ciardullo, R., Jacoby, G. H., & Harris, W. E. 1991, ApJ, 383, 487
de Vaucouleurs, G. 1960, ApJS, 5, 233
———. 1983, ApJ, 268, 451
———. 1992, personal communication

de Vaucouleurs, G. 1993a, ApJ, 415, 10
———. 1993b, ApJ, 415, 33
de Vaucouleurs, G., de Vaucouleurs, A., Corwin, H. G., Buta, R. J., Paturel, G., & Fouque, P. 1991, Third Reference Catalogue of Bright Galaxies (3d ed.; New York: Springer-Verlag)
de Vaucouleurs, G., & Olson, D. W. 1982, ApJ, 256, 346
Faber, S. M., Balick, B., Gallagher, J. S., & Knapp, G. R. 1977, ApJ, 214, 383
Faber, S. M., & Burstein, D. 1988, in Large-Scale Motions in the Universe, ed. V. C. Rubin & G. V. Coyne, S. J. (Princeton: Princeton Univ. Press), 115
Ford, H. C., Ciardullo, R., Jacoby, G. H., & Hui, X. 1989, in IAU Symp. 131, Planetary Nebulae, ed. S. Torres-Peimbert (Dordrecht: Reidel), 335
Ford, H. C., & Jenner, D. C. 1979, BAAS, 10, 665
Forman, W., Jones, C., & Tucker, W. 1985, ApJ, 293, 102
Freedman, W. L., & Madore, B. F. 1990, ApJ, 365, 186
Huchra, J. P. 1985, in The Virgo Cluster of Galaxies, ed. O.-G. Richter & B. Binggeli (Garching: ESO), 181
Huchra, J. P., & Geller, M. J. 1982, ApJ, 257, 423 (HG82)
Hui, X. 1992, Ph.D. thesis, Bost Univ.
Hui, X., Ford, H. C., Ciardullo, R. C., & Jacoby, G. 1993a, ApJ, 414, 463
———. 1993b, ApJS, 88, 423
Hui, X., Ford, H. C., Freeman, K. C., & Dopita, M. A. 1995, ApJ, in press
Jacoby, G. H., Ciardullo, R., & Ford, H. C. 1990, ApJ, 356, 332 (J90)
Jacoby, G. H., Ciardullo, R., Ford, H. C., & Booth, J. 1989, ApJ, 344, 704
Jacoby, G. H., Quigley, R. J., & Africano, J. L. 1987, PASP, 99, 672
Jacoby, G. H., Walker, A. R., & Ciardullo, R. 1990, ApJ, 365, 471
Jarvis, B. J., & Freeman, K. C. 1985, ApJ, 295, 324
Kormendy, J., & Illingworth, G. 1982, ApJ, 256, 460
Kormendy, J., & Westpfahl, D. J. 1989, ApJ, 338, 752
McMillan, R., Ciardullo, R., & Jacoby, G. H. 1993, ApJ, 416, 62
Rubin, V. C., Burstein, D., Ford, W. K., & Thonnard, N. 1985, ApJ, 289, 81
Sandage, A., & Tammann, G. A. 1981, A Revised Shapley-Ames Catalog of Bright Galaxies (2d ed.; Washington, DC: Carnegie Inst. of Washington)
Schechter, P. L. 1980, AJ, 85, 801
Schweizer, F. 1978, ApJ, 220, 98
Seaton, M. J. 1979, MNRAS, 187, 73P
Secker, J., & Harris, W. E. 1993, AJ, 105, 1358
Stetson, P. B. 1989, Highlights Astron., 8, 635
Stone, R. P. S., & Baldwin, J. A. 1983, MNRAS, 204, 347
Tammann, J. L. 1992, personal communication
Tully, R. B. 1987, ApJ, 321, 280 (T87)
Wainscoat, R. J., Hyland, A. R., & Freeman, K. C. 1990, ApJ, 348, 85
Welch, D. L., McAlary, C. W., McLaren, R. A., & Madore, B. F. 1986, ApJ, 305, 583
Wirth, A. 1981, AJ, 86, 981